Developing synergy regression models with space-borne ALOS PALSAR and Landsat TM sensors for retrieving tropical forest biomass

Suman Sinha[1,*], C Jeganathan[1], L K Sharma[2], M S Nathawat[3], Anup K Das[4] and Shiv Mohan[5]

[1]*Department of Remote Sensing, Birla Institute of Technology, Mesra, Ranchi 835 215, Jharkhand, India.*
[2]*Department of Environmental Science, School of Earth Sciences, Central University of Rajasthan, Bandarsindri 305 817, Ajmer, Rajasthan, India.*
[3]*School of Sciences, Indira Gandhi National Open University (IGNOU), Maidan Garhi, New Delhi 110 068, India.*
[4]*Space Application Centre (ISRO), Department of Space, Government of India, Jodhpur Tekra, Satellite Road, Ahmedabad 380 015, Gujarat, India.*
[5]*PLANEX, Physical Research Laboratory, Thaltej Campus, Ahmedabad 380 059, Gujarat, India.*
[*]*Corresponding author. e-mail: sumanrumpa.sinha@gmail.com*

Forest stand biomass serves as an effective indicator for monitoring REDD (reducing emissions from deforestation and forest degradation). Optical remote sensing data have been widely used to derive forest biophysical parameters inspite of their poor sensitivity towards the forest properties. Microwave remote sensing provides a better alternative owing to its inherent ability to penetrate the forest vegetation. This study aims at developing optimal regression models for retrieving forest above-ground bole biomass (AGBB) utilising optical data from Landsat TM and microwave data from L-band of ALOS PALSAR data over Indian subcontinental tropical deciduous mixed forests located in Munger (Bihar, India). Spatial biomass models were developed. The results using Landsat TM showed poor correlation ($R^2 = 0.295$ and RMSE = 35 t/ha) when compared to HH polarized L-band SAR ($R^2 = 0.868$ and RMSE = 16.06 t/ha). However, the prediction model performed even better when both the optical and SAR were used simultaneously ($R^2 = 0.892$ and RMSE = 14.08 t/ha). The addition of TM metrics has positively contributed in improving PALSAR estimates of forest biomass. Hence, the study recommends the combined use of both optical and SAR sensors for better assessment of stand biomass with significant contribution towards operational forestry.

1. Introduction

Land and forest cover dynamics are important parameters in current strategies and policies for forest management and vegetation monitoring (Sinha *et al.* 2015a). Proper enumeration of biomass and carbon is a preliminary requirement for monitoring reducing emissions from deforestation and forest degradation (REDD) (Gibbs *et al.* 2007; Sharma *et al.* 2013; Sinha and Sharma 2013). The largest pool of carbon is stored as aboveground living biomass of trees that suffers deforestation and degradation (Kumar *et al.* 2011). There is a need to measure the forest biophysical and structural properties that characterizes the forest vegetation and influences the biomass/carbon stock (Mbaabu *et al.* 2014). Accurate reliable estimation of global forest cover with biomass/carbon sequestered in earth's

Keywords. ALOS PALSAR; Landsat TM; polarization; backscatter; tropical deciduous forest; biomass; Munger; Bihar.

J. Earth Syst. Sci., DOI 10.1007/s12040-016-0692-z, **125**, No. 4, June 2016, pp. 725–735

forests is mandatory for understanding the global carbon budget (DeFries *et al.* 2007).

There are numerous methods for the assessment of tropical forest biomass or carbon stock documented in literatures (Gibbs *et al.* 2007; Goetz *et al.* 2009), of which forest inventorization based on field measurements via destructive sampling is the most accurate and reliable (Goetz *et al.* 2009). Also, the use of allometric equations to extrapolate plot values to forest stands (Lu 2006) is widely recommended. On the contrary, this method is costly, arduous, time extensive, non-spatial, and difficult to be applied to a large extent in remote inaccessible areas, specifically over tropical forests (Englhart *et al.* 2011, 2012). Goetz *et al.* (2009) suggested the biome approach as an indirect method to enumerate biomass that requires inputs of land cover map and forest type specific biomass values.

Satellite plays a vital role for global forest biomass/carbon stock assessments (Gibbs *et al.* 2007). Lu (2006) emphasized on the use of satellites for measuring and monitoring biomass. The limitations of the *in-situ* study are overcome by using remote sensing satellites with further added advantages like wide range of spatial, spectral and temporal resolutions of the satellite data. Remote sensing technology when supplemented with *in-situ* measurements provides precise and easy assessment of biomass or carbon stock (Rosenqvist *et al.* 2003). Optical sensors using spectral-based approaches are frequently used for biomass assessment (Lu 2005, 2006; Singh *et al.* 2006; Kale *et al.* 2009; Kumar *et al.* 2013; Sharma *et al.* 2013), though facing several drawbacks like occurrence of clouds and early saturation of the spectral bands that hampers the biomass estimation process (Gibbs *et al.* 2007). Kale *et al.* (2009) used multi-sensor multi-temporal optical data for carbon sequestration study. However, the inability of the electromagnetic waves operating in the optical region to penetrate the canopy makes the approach ineffective for estimating the bole biomass which contributes maximum towards the overall aboveground biomass. This drawback is surmounted by Synthetic Aperture Radar (SAR) that not only has the intrinsic capability to penetrate the canopy but also the clouds; hence is weather-independent. Along with this, SAR interactions are sensitive to wave polarization, target dielectric constant, surface roughness, wave incident angles, etc. (Sinha *et al.* 2015b). Biomass estimation using SAR also depends on these parameters. These potentialities are exploited for retrieval of tropical forest biomass (Kuplich *et al.* 2005; Gama *et al.* 2010; Alappat *et al.* 2011; Englhart *et al.* 2011, 2012; Sharma *et al.* 2014; Sinha *et al.* 2015c). Longer SAR wavelengths (L- and P-band) with cross-polarizations (HV and VH) are more sensitive to biomass than short wavelengths (X- and C-band) with HH or VV co-polarizations (Dobson *et al.* 1992; Hamdan *et al.* 2011; Wollersheim *et al.* 2011; Sharma *et al.* 2014; Sinha *et al.* 2015b).

The saturation level improves while using SAR, though the problem remains. A way to reduce the problem of saturation is to use integrated multi-source remote sensing data. Data from more than one sensor reduce the uncertainty related to a single sensor (Sarker 2010). Several studies have used multiple remote sensing data to accurately estimate the forest biophysical parameters. For example, Mbaabu *et al.* (2014) used optical GeoEye-1 and LiDAR; Alappat *et al.* (2011) used SAR C- and L-bands and Englhart *et al.* (2011) used SAR X- and L-bands; while Sarker (2010) used both multi-sensor optical (SPOT-5 and AVNIR-2) and SAR (PALSAR and Radarsat-2) data. Hyde *et al.* (2006, 2007) used multi-sensor synergy of optical, SAR, InSAR and LiDAR for assessment of AGB.

Optical data are useful in foliar biomass estimations while SAR backscattering is sensitive to woody biomass (Dobson *et al.* 1992; Sarker 2010). Hence, the current study targets in the integrated use of optical Landsat TM and SAR L-band ALOS PALSAR data to develop regression models to predict AGB with the integration of field data over deciduous tropical mixed forests located in Munger, India. The method applied can serve as a potential benchmark for calculating biomass in the complex set-up of the tropical forest system where field experiments are difficult to carry out.

2. Material and methods

2.1 *Study area*

The tropical mixed deciduous forests found over the Munger region of Bihar, India is taken as the study area (figure 1). The area lies within the geographic extent of 25°19′30″–24°56′50″N latitude and 86°33′33″–86°11′51″E longitude, covering an area of approx 672.5 km^2. With more than 89% of the area under forests, mainly open and degraded, the floral diversity comprises of *Shorea robusta*, *Acacia catechu*, *Madhuca longifolia*, *Dendrocalamus strictus*, *Diospyros melanoxylon* and *Terminalia tomentosa* as the dominant floral species (Sinha *et al.* 2013). The forests suffer from limited anthropogenic activities like settlements, mining activities, agricultural development and plantations. These virgin forests serve as ideal set-up for carrying out the experiment with limited ground data. Two remote sensing data are used; out of which one is optical satellite sensor of Landsat TM and the other is L-band SAR sensor of Fine Beam Dual (FBD) HH/HV polarized ALOS PALSAR. The

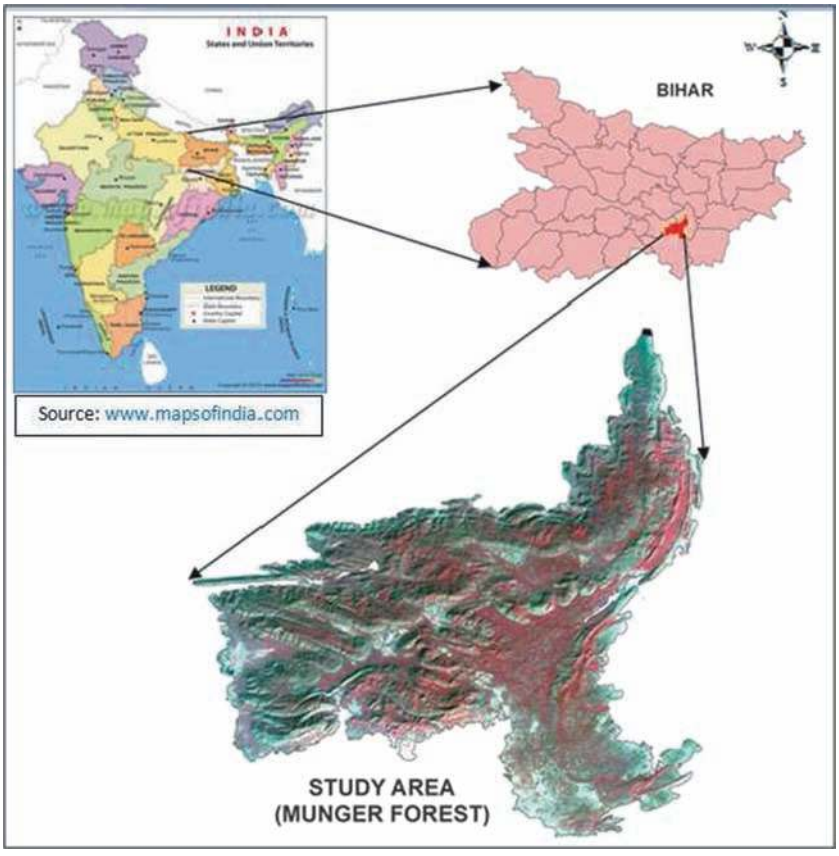

Figure 1. Location map of the study area.

Table 1. *Satellite data specifications.*

Remote sensing data type	Optical	SAR
Satellite	Landsat 5	ALOS
Sensor	TM	PALSAR
Launching country (Organization)	USA (NASA)	Japan (JAXA)
Date of launch	1st March, 1984	24th January, 2006
Spatial resolution	30 m (thermal 120 m)	25 m
Swath width	185 km	70 km (34.3° incident angle)
Wavelengths	B1: 0.45–0.52 μm	L-band; 15–30 cm
	B2: 0.52–0.60 μm	Fine Beam Dual (HH/HV)
	B3: 0.63–0.69 μm	
	B4: 0.76–0.90 μm	
	B5: 1.55–1.75 μm	
	B6: 10.4–12.5 μm	
	B7: 2.08–2.35 μm	
Year of data acquisition	2010	2010
Source of data acquisition	USGS (http://glovis.usgs.gov/), USA	JAXA, Japan

specifications of the data are documented in table 1. Figure 2 describes the approach by which these data are used singly and in combination to develop multiple linear regression (MLR) model to predict AGB, with inputs of the primary data as generated from the field.

2.2 *Field data collection*

Field inventory is made by making direct *in-situ* field calculations. The primary data such as forest types, forest density, species composition, stand height, and girth at breast height (GBH) are

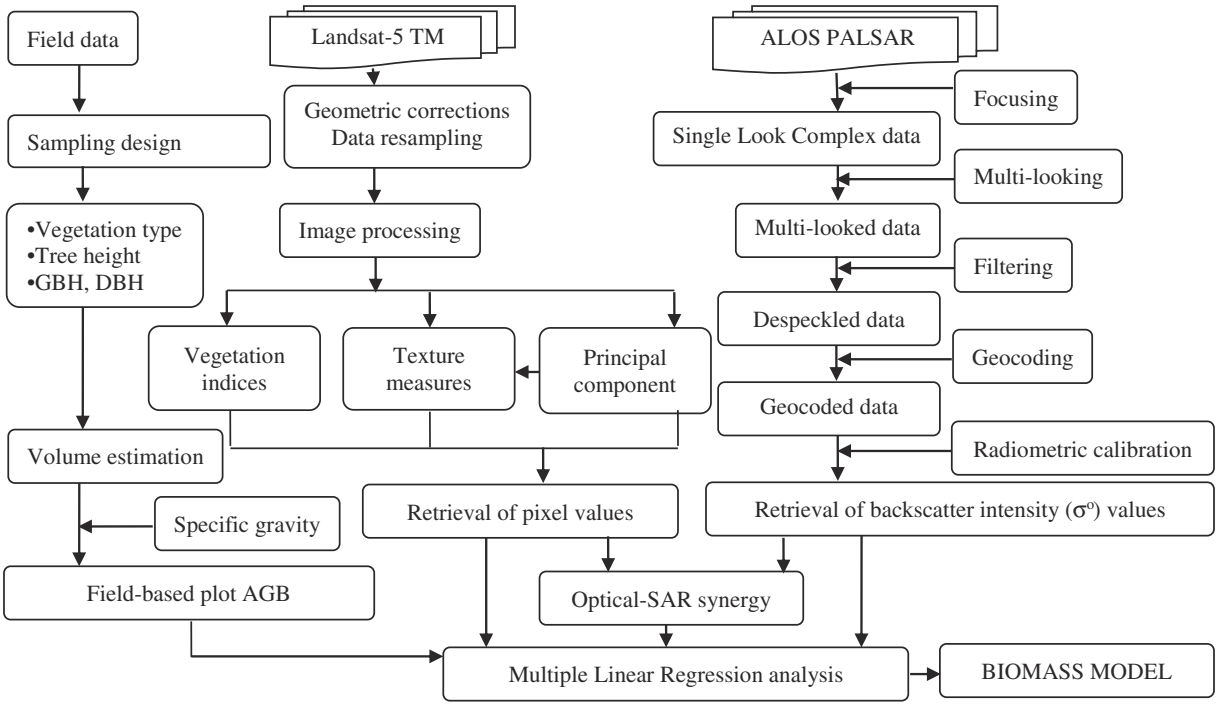

Figure 2. Methodology flowchart.

essential to estimate AGB; these information are collected through the random sampling during 2010–2011. Another utility of the ground truth was to get accurate information regarding the land use and land cover of the area. Considering the variability and inaccessibility of the study area, a total of 34 square sample plots representing homogeneous vegetation units, with an area of 0.1 hectare (Singh *et al.* 2006; Sinha and Sharma 2013) each were selected from every forest type and density classes present in the study area; hence covering 0.005% of the total forest area. Considering the time availability and complicacy of the study, it has been proposed that the required sample size can vary between 0.001% and 0.005% of the total study area (Kale *et al.* 2009). The 0.1 hectare sample plots resulted in the plot dimensions almost equal to the pixel size of the satellite data, thus the plot size is justified *vis-à-vis* satellite sensor resolution (Sinha and Sharma 2013). The sample point distribution was designed considering that they provided ample representation of the different strata of the forest with easy approachability and feasibility of taking multi-time observations. In each plot, GBH (Girth at Breast Height) of each adult individual tree (>30 cm GBH) was measured at 1.37 m from the ground level using measuring tape. GBH was converted to DBH (Diameter at Breast Height) by dividing the value of GBH with 3.14 (Sinha and Sharma 2013). Using the tree DBH and height information, the tree volumes were estimated via volumetric equations (FSI 1996) and biomass were calculated after multiplying each tree volume with the respective specific gravity (FRI 1996). These individual biomass values were added together to calculate the individual sample plot biomass. A sample of 30 or more statistically represents normal distribution of any sampling (Singh *et al.* 2006).

2.3 *Landsat TM derived metrices*

Lu (2005) has used Landsat TM data to estimate the above ground biomass in the tropical Amazonian forests. In this study, the TM imagery is geometrically rectified and co-registered in reference to already registered Landsat ETM+ and IRS P6 LISS-III image of the same region, which were inturn co-registered with the Survey of India (SOI) toposheet considering analogous distinct identifiable objects on the toposheets, ground and image (Sinha *et al.* 2013, 2014). The geocoded TM image had UTM projection, WGS-84 datum and Zone 45 North on a 1:50,000 scale. Principal components, texture measures and NDVI (NIR−red/NIR+red) were calculated at the stand level for the image. NDVI is observed to bear the strongest relationship with the biomass among all the vegetation indices (Sarker 2010; Kumar *et al.* 2013; Sharma *et al.* 2013). Texture measures obtained through occurrence matrices were performed using 3×3 window size for individual bands of Landsat TM. Simultaneously, texture measures of principal components using 3×3 window size were analyzed.

2.4 *PALSAR backscatter retrieval*

The raw Single Look Complex (SLC) SAR imagery was converted to backscatter intensity data. The data was properly calibrated and preprocessed prior to its use for biomass retrieval. The preprocessing of the ALOS PALSAR data was performed in a sequence of steps in SARScape software. The conversion of slant range image to ground range image marks the initial step which is crucial for removing the slant range distortions producing SLC data in range with equal pixel spacing. Next, multi-looking of the SLC was done to convert the data in complex format to real number format (i.e., power or intensity). This step also reduces the speckles present in the SLC image. Seven azimuth looks for one look in the range were selected for multi-looking that resulted in almost square pixels in the image. The data in complex number format was converted to amplitude and then to power images respectively resulting in a floating point image representing the power of an amplitude image with pixel values having real values. Next, using the satellite orbital parameters, the image was geocoded and rectified to remove the geometric errors, which was done with SRTM DEM resampled by nearest neighbourhood method to 30 m pixel size and reprojected to UTM-WGS84 coordinate system. Thereafter, radiometric calibration was carried out using equation (1) which marks the conversion of power image to linear backscatter image and then to decibel image.

$$\sigma^0 = 10 * a \log 10(DN) + A_0 \qquad (1)$$

where σ^0 = backscatter coefficient or sigma nought values in decibles (dB), DN=power (or intensity) image, A_0 (sensor calibration factor) = –115 dB.

Speckles in the imagery were reduced after radiometric calibration. This can cause alterations in the backscatter values. As the models developed are dependent on the backscatter values, the alterations in the values are not desirable. Henceforth, mean filters with 3×3 window size (moving window of a few pixels) was adopted for the study. The use of SAR-specific filters with varying window size was avoided in the study as that would surely lead to more clarity and smoothing of the SAR image features by effectively suppressing the speckles, but at the expense of information loss in terms of backscatter values. Both multi-look processing and spatial filtering reduce speckle at the cost of resolution. Therefore, the amount of speckle reduction desired must balance the applications and necessary information.

2.5 *MLR spatial modelling*

Backscatter coefficients generated from SAR data derived in equation (1) and the metrics generated from Landsat TM were equated to the field-based plot AGB values. The values were statistically integrated using Multiple Linear Regression (MLR) analysis to find the best fit model that improved the accuracy of the model estimates. The performance of the model estimates were calculated based on correlation coefficient (R) and coefficient of determination (R^2) values, that are derived from correlation between estimated (field-based) and predicted (modelled) AGB and the RMSE (root mean square error) of the estimates. AGB maps were generated using the models designed in GIS framework.

2.6 *Model evaluation*

Uncertainty in the assessment of biomass with geospatial approach was analyzed using a wide range of statistical metrices, like R^2, RMSE, MAD, MBE, NDRMSE, NDMAD, NDMBE and absolute accuracy. These metrices were used to compare and evaluate the performance of the spatial biomass models generated through MLR modelling.

1. Coefficient of determination (R^2):

$$R^2 = \left[\frac{\sum \left(Y_f - \overline{Y}_f\right)\left(Y_m - \overline{Y}_m\right)}{\sqrt{\sum \left(Y_f - \overline{Y}_f\right)^2 \left(Y_m - \overline{Y}_m\right)^2}} \right]^2$$

2. Root mean square error (RMSE):

$$\text{RMSE} = \sqrt{\left[\frac{\sum \left(Y_m - Y_f\right)^2}{N} \right]}$$

3. Mean absolute deviation (MAD):

$$\text{MAD} = \frac{\sum |Y_m - Y_f|}{N}$$

4. Mean bias error (MBE):

$$\text{MBE} = \frac{\sum \left(Y_m - Y_f\right)}{N}$$

5. Non-dimensional RMSE (NDRMSE):

$$\text{NDRMSE} = \frac{\sum \left[(Y_m - Y_f)/Y_f\right]^2}{N}$$

6. Non-dimensional MAD (NDMAD):

$$\text{NDMAD} = \frac{\sum |[(Y_m - Y_f)/Y_f]|}{N}$$

7. Non-dimensional MBE (NDMBE):

$$\text{NDMBE} = \frac{\sum [(Y_m - Y_f)/Y_f]}{N}$$

8. Average Absolute Accuracy (ζ):

$$\zeta = \left[1 - \frac{1}{N} \sum \frac{|Y_m - Y_f|}{Y_f}\right] * 100$$

where Y_f = value generated from field, Y_m = value generated through model, $\overline{Y_f}$ = average of Y_f values, $\overline{Y_m}$ = average of Y_m values, N = number of study sites.

2.7 *Model validation*

The models (A, B and C) developed were statistically validated with nine additional field AGB data of year 2015 and the corresponding aforesaid statistical measures were executed. However, these conventional statistical measures are seldom optimal for evaluating the agreement (or disagreement) between the modelled and the actual field data. Henceforth, a non-dimensional statistical measure, namely Willmott's index of agreement (d) was simultaneously used. This overcomes and circumvents the disadvantages of the aforesaid statistical metrices and is more suitable for investigating model validation, where comparison between the observed and model-predicted values need to be executed; with an assumption that the observed data are completely error-free and hence can be purely treated as reference for the comparison (Ji and Gallo 2006).

Willmott's Index of agreement (d):

$$d = 1 - \frac{\sum (Y_f - Y_m)^2}{\sum \left(\left|Y_f - \overline{Y_f}\right| + \left|Y_m - \overline{Y_f}\right|\right)^2},$$

where Y_f = field generated value, Y_m = model generated value, $\overline{Y_f}$ = average of Y_f values.

3. Results and discussion

3.1 *Descriptive statistics of sampling plots*

Table 2 documents the descriptive statistics of the AGB measured on ground for the 34 sample plots. The AGB for plots ranged from 11.35 to 172.07 t/ha with an average value of 72.94 t/ha and standard deviation (SD) of 41.15 t/ha. The high SD indicates that the data points are spread out over a large range of values and the sample has large variation of data.

Table 2. *Statistical characteristics of sampling plots.*

Parameter	AGB (t/ha)
Maximum	172.0729
Minimum	11.3533
Mean	72.9469
Standard deviation	41.1525
Standard variance	1693.532
Number of plots	34

3.2 *Model development*

Relationship between the field generated AGB with both the corresponding SAR backscattering coefficients and TM derived metrices were examined separately. On regressing NDVI values generated from the optical imagery to the plot AGB, a maximum correlation (R^2) of 0.26 was obtained following linear model as the best fit (table 3). Equation (2) thus developed from the relation between plot AGB and NDVI is used as a component in the final synergic model for AGB assessment:

$$\text{AGB} = 340.13 * \text{TM}_{\text{NDVI}} - 143.09 \qquad (2)$$

Texture measures obtained through occurrence matrices were performed with 3×3 window size for individual bands of TM datasets. The highest R^2 value was obtained for the texture measure variance of TM band 4. Equation (3) thus developed from the relation was used as a component in the final synergic model for AGB assessment:

$$\text{AGB} = 81.811 * e^{(-0.056 * \text{TM}_{\text{B4variance}})} \qquad (3)$$

PCA and texture measures of PCA components with 3×3 window size were analyzed. Relationships between the first four components of PCA were investigated with the plot AGB. The first few components harboured most of the information, specifically, the first component that gave the direction of the maximum spread of the data. The greatest correlation of plot AGB was observed with the first principal component (PCA1) variance in logarithmic model. Equation (4) thus developed from the relation was used as a component in the final synergic model for AGB assessment:

$$\text{AGB} = 76.766 * e^{(-0.003 * \text{TM}_{\text{PCA1variance}})} \qquad (4)$$

Equations (2, 3 and 4) were statistically combined in MLR to obtain the best fit integrated model

Table 3. *Correlation (R^2) between NDVI to the plot AGB.*

Relation	R^2
Linear	0.2648
Logarithmic	0.2534
Exponential	0.2320
Power	0.2297

(equation 5) of metrices derived from Landsat TM data, thus representing the AGB prediction model generated from optical satellite data.

$$\begin{aligned}\text{AGB} = {} & 289.1105 * \text{TM}_{\text{NDVI}} \\ & + 54.2652 * e^{(-0.056 * \text{TM}_{\text{B4variance}})} \\ & - 20.6116 * e^{(-0.003 * \text{TM}_{\text{PCA1variance}})} \\ & - 136.306 \end{aligned} \quad (5)$$

SAR polarization is sensitive to the size, shape and orientation of scattering elements and this is responsible for depolarization or attenuation of the backscattered signals. SAR backscatter coefficient values extracted from FBD ALOS PALSAR were correlated to the plot AGB and the R^2 values are documented in table 4. The backscatter coefficients generally range between −14 and −1 in forested areas for HH polarization and −25 to −7 for HV polarization (figure 3). Hence, higher values are exhibited by HH polarization followed by HV polarization; however, the range of backscatter values is greater for HV polarization. The HV cross-polarized image provides better visual discrimination of forest and non-forest areas than the HH co-polarized image. In contrast, HH polarization has the greatest interaction with the trunk due to its vertical structure and hence, most sensitive towards the bole AGB. In this study, HH polarization shows better correlation of 0.849 than HV polarization with $R^2 = 0.564$. Therefore, equation (6) was developed from the relation between AGB and HH polarized ALOS PALSAR data to be used as a component in the final synergic model for AGB assessment.

$$\text{AGB} = 1067.3 * e^{(0.2765 * \sigma^{\circ}_{L\_\text{HH}})} \quad (6)$$

Figure 3 depicts the relationship between the field calculated AGB and the metrices derived from optical and SAR sensors. The equations used as inputs in the synergic model for predicting biomass are presented in the figure.

Table 4. *Correlation coefficient (R^2) between SAR backscatter coefficient and biomass.*

ALOS PALSAR polarization	HH	HV
Correlation coefficient (R^2)	0.8490	0.5645

3.3 *Synergy regression modelling*

It is recommended that all the points be used for developing the prediction models to enhance and improve the robustness of the models. Equations (2, 3, 4) (integrated as equation 5) and (6) were statistically combined in MLR to find the best fit model and the final prediction synergy model is represented in equation (7).

$$\begin{aligned}\text{AGB} = {} & 117.821 * \text{TM}_{\text{NDVI}} \\ & + 18.9965 * e^{(-0.056 * \text{TM}_{\text{B4variance}})} \\ & - 37.4387 * e^{(-0.003 * \text{TM}_{\text{PCA1variance}})} \\ & + 918.6251 * e^{(0.2765 * \sigma^{\circ}_{L\_\text{HH}})} \\ & - 47.6045 \end{aligned} \quad (7)$$

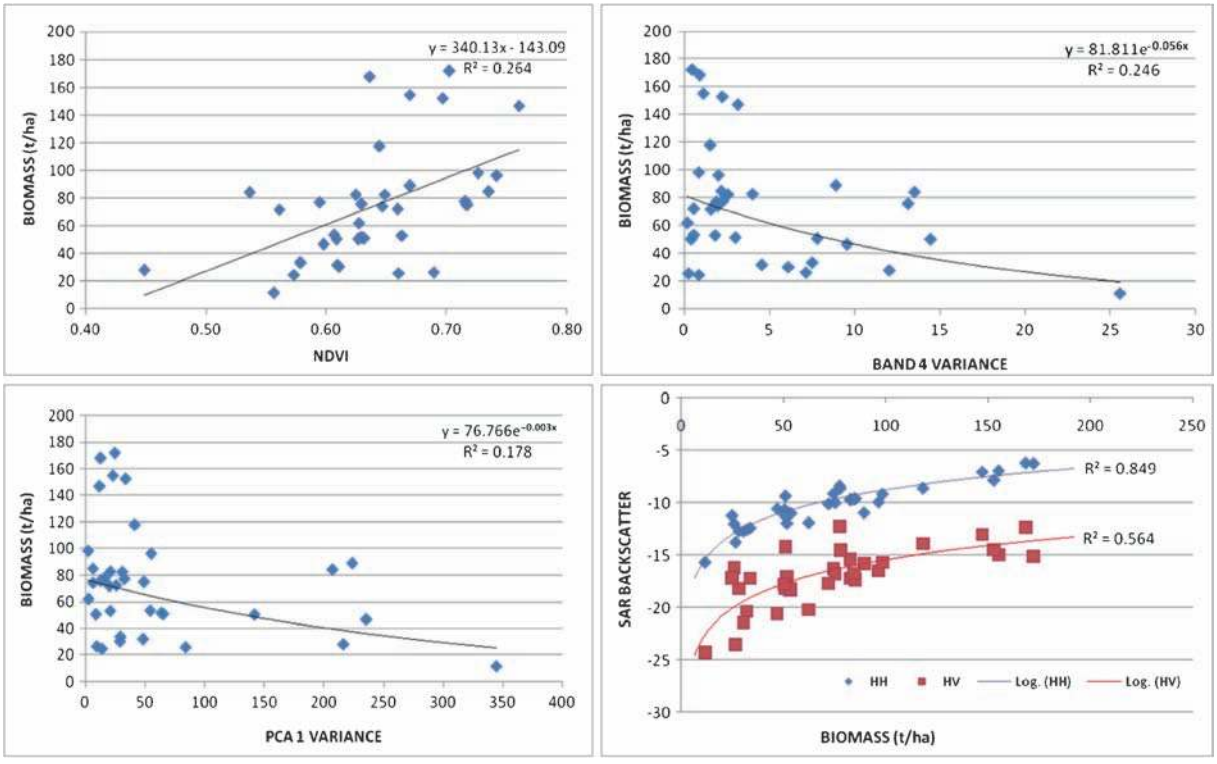

Figure 3. Relationship between the field AGB and the metrices derived from optical and SAR sensors.

3.4 *Model performance evaluation*

Evaluation of the model performance signifies the comparison among the different models developed and their accuracy in predicting the AGB. The parameters for determining the accuracy of the models are already detailed before and the corresponding values for the models generated are mentioned in table 5. Here the comparison is among the models generated as equations (5) (Model A), (6) (Model B) and (7) (Model C). 'Model A' shows weak correlation of 0.295 with high RMSE of 35 t/ha and the model accuracy is only 47.54%. In contrary, 'Model B' had the highest accuracy of 80.61%, with high correlation of 0.868 and low RMSE of 16.06 t/ha. However, the integrated optical-SAR model ('Model C') showed the best results, with highest correlation of 0.892 and least RMSE of 14.08 t/ha. Also, the table indicated low MAD and MBE values for 'Model C'. With a significantly high model accuracy of 78.73%, 'Model C' is considered the best model out of the three for predicting AGB (see table 5 and figure 4). Figure 4 represents the relationship between the field-estimated AGB (observed) and modelled (predicted) AGB. Simultaneously, figure 5 illustrates the comparison of the model evaluation statistical metrices among all the three models, which summarizes the fact that 'Model C', i.e., optical

Table 5. *Model evaluation parameters for biomass prediction.*

AGB Model	A (optical)	B (SAR)	C (optical + SAR)
R^2	0.295	0.868	0.892
RMSE (t/ha)	35.002	16.063	14.081
NDRMSE	0.598	0.073	0.104
MAD	28.058	12.449	11.279
NDMAD	0.525	0.194	0.213
MBE	0.000	−1.109	0.000
NDMBE	0.272	0.032	0.074
Av. abs. accuracy	47.537	80.605	78.725

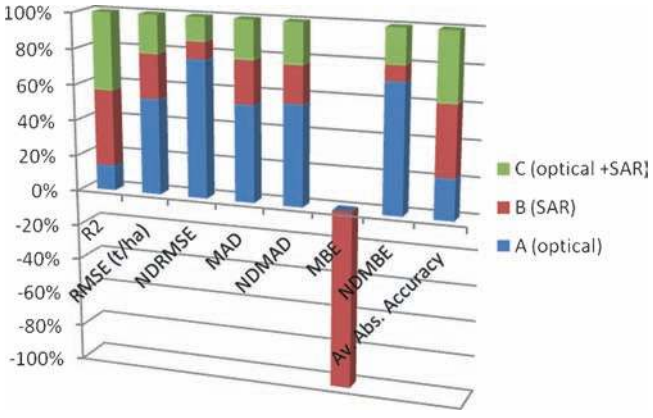

Figure 5. Statistical comparisons of AGB models.

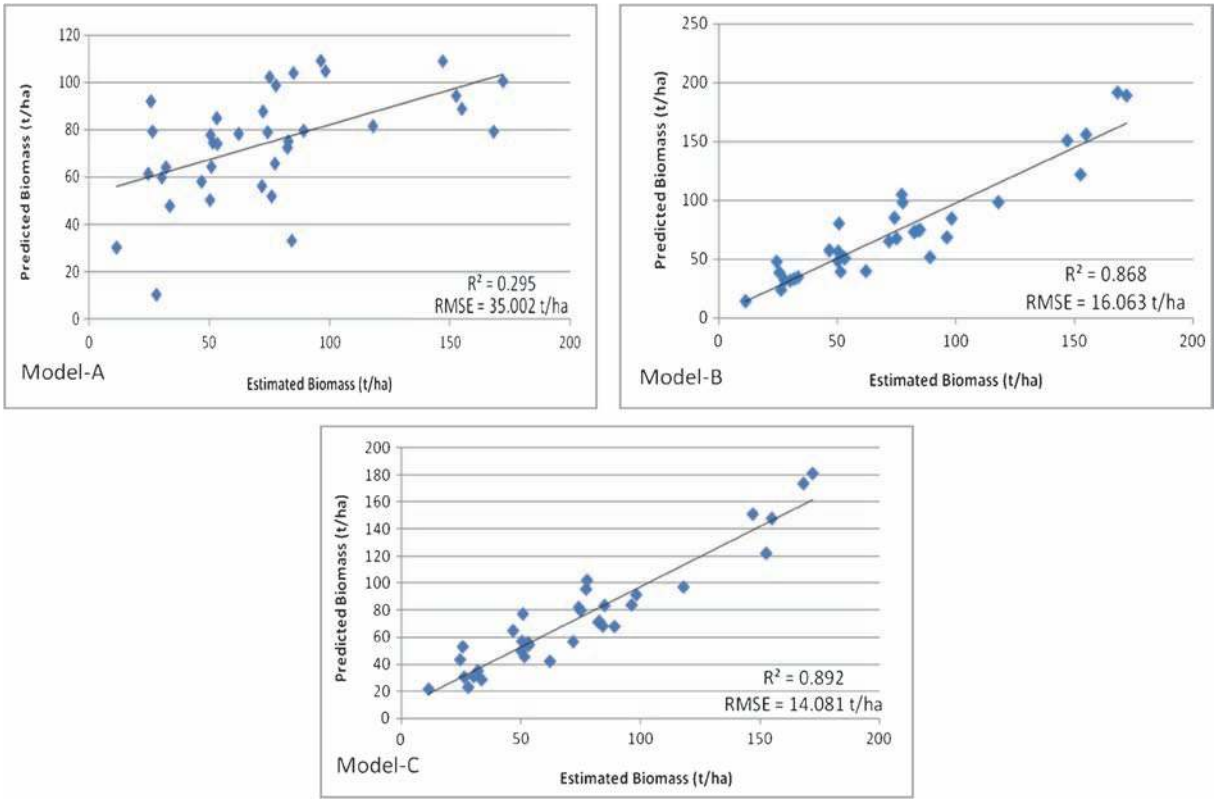

Figure 4. Relationship between the field-estimated and modelled (predicted) biomass.

and SAR integrated approach provides the best technique for enumeration and assessment of AGB. The models (A, B and C) were further validated with additional nine AGB sample plots and the results are presented in table 6. The table reveals the better acceptability of 'Model C' for AGB assessment in comparison to 'Models A and B'. The value of 'd' is more nearing to '1' in case of 'Model C' than the other two models (A and B) which means that the modelled values fit the observed values better, and hence, shows greater agreement. The R^2, RSME and model accuracy values show similar inferences. Thus, it can be concluded that Model C is the most accurate model and hence acceptable for AGB assessment. Figure 6 portrays the biomass map derived from 'Model C' which clearly shows that the less vegetative parts surrounding the boundary of the study area, water bodies and the built-up regions (in the periphery and at the central parts) are represented by low biomass class (i.e., <25 t/ha). Maximum portion of the forested region is covered under the range of 25–75 t/ha of biomass. Most of the high density vegetation seems to have biomass ranging from 75–125 t/ha, usually present in the interior parts of the study area. It can be also observed that the early saturation of biomass with the use of optical data alone can be counteracted with the integrated use of both optical and SAR data due to the better

Table 6. *Model validation: Comparison between AGB models.*

AGB Model	A (optical)	B (SAR)	C (optical + SAR)
R^2	0.574	0.713	0.769
RMSE (t/ha)	26.736	22.340	17.151
NDRMSE	0.932	0.216	0.065
MAD	23.227	19.669	14.350
NDMAD	0.637	0.382	0.214
MBE	14.652	−12.281	−3.906
NDMBE	0.559	−0.085	−0.039
Av. abs. accuracy	36.305	61.768	78.555
Willmott's index (d)	0.722	0.883	0.931

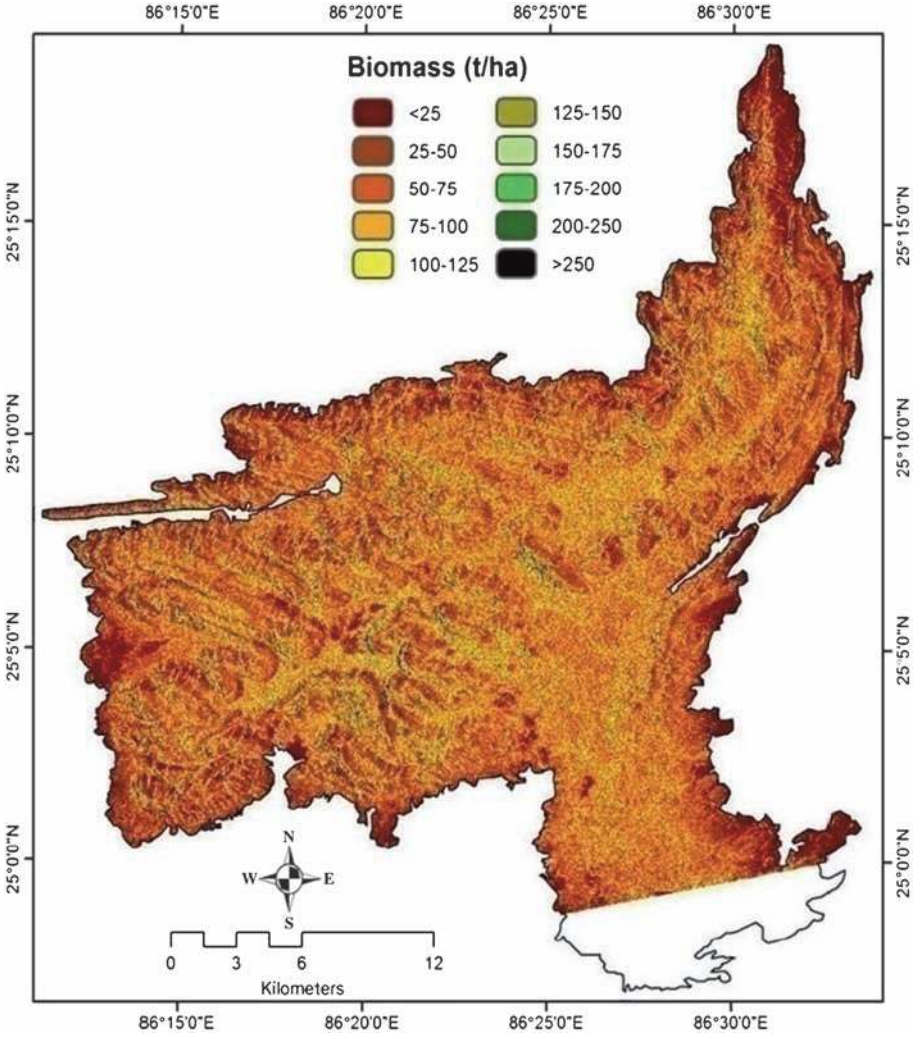

Figure 6. Biomass map of the study area.

relationship of the biomass to the L-band SAR backscatter (figures 3, 4 and 5; table 5). Hence, the integrated optical-SAR model provided the most accurate result for predicting biomass (or AGB).

4. Conclusions

The concept of REDD is gaining momentum among all the forest management practices that affect the carbon/biomass stock of forests. This is specifically important for tropical forest as the assessment is complex in such heterogeneous forest landscapes. The relationship between L-band ALOS PALSAR backscatter coefficient and forest biomass has been established in the present study. In a comparison between the optical and SAR data, the SAR data is observed to produce much better and accurate estimates of the forest biomass. The synergic use of optical and SAR satellite remote sensing data has been successfully illustrated in this study. The integrated use of multi-sensor data thus showcases an easy and effective way to improve the accuracy of biomass estimates; even if with limited field data.

Acknowledgements

The authors sincerely acknowledge JAXA (Japan Aerospace Exploration Agency, Japan) for providing the ALOS PALSAR data under ALOS RA-4 project. We sincerely acknowledge Space Application Centre (SAC, ISRO), Ahmedabad (India), for providing facilities to process the PALSAR data. The authors express sincere gratitude to the Department of Science and Technology (DST), Government of India for providing funds under DST-INSPIRE Program (Ref. No. DST/INSPIRE FELLOWSHIP/2010/[316]) to carry out the research to Suman Sinha.

References

Alappat V O, Joshi A K and Krishnamurthy Y V N 2011 Tropical dry deciduous forest stand variable estimation using SAR data; *J. Indian Soc. Remote Sens.* **39(4)** 583–589.

DeFries R, Achard F, Brown S, Herold M, Murdiyarso D, Schlamadinger B and deSouza C Jr 2007 Earth observations for estimating greenhouse gas emissions from deforestation in developing countries; *Environ. Sci. Policy* **10** 385–394.

Dobson M C, Ulaby F T, Le Toan T, Beaudoin A, Kasischke E S and Christensen N 1992 Dependence of radar backscatter on coniferous forest biomass; *IEEE Trans. Geosci. Remote Sens.* **30** 412–415.

Englhart S, Keuck V and Siegert F 2011 Aboveground biomass retrieval in tropical forests – the potential of combined X- and L-band SAR data use; *Remote Sens. Environ.* **115** 1260–1271.

Englhart S, Keuck V and Siegert F 2012 Modelling aboveground biomass in tropical forests using multi-frequency SAR data – a comparison of methods; *IEEE J. Sel. Topics Appl. Earth Observ.* **5(1)** 298–306.

FRI 1996 *Indian Woods*; Forest Research Institute, Dehradun.

FSI 1996 *Volume equations for forests of India, Nepal and Bhutan*; Forest Survey of India, Ministry of Environment and Forests, Govt. of India, Dehradun.

Gama F F, dos Santos J R and Mura J C 2010 Eucalyptus biomass and volume estimation using interferometric and polarimetric SAR data; *Remote Sens.* **2** 939–956.

Gibbs H K, Brown S, Niles J O and Foley J A 2007 Monitoring and estimating tropical forest carbon stocks: Making REDD a reality; *Environ. Res. Lett.* **2** 1–13.

Goetz S J, Baccini A, Laporte N T, Johns T, Walker W, Kellndorfer J, Houghton R A and Sun M 2009 Mapping and monitoring carbon stocks with satellite observations: A comparison of methods; *Carbon Balance Manag.* **4(2)** 1–7.

Hamdan O, Aziz H K and Abd Rahman K 2011 Remotely sensed L-band SAR data for tropical forest biomass estimation; *J. Trop. For. Sci.* **23(3)** 318–327.

Hyde P, Dubayah R, Walker W, Blair J B, Hofton M and Hunsaker C 2006 Mapping forest structure for wildlife habitat analysis using multi-sensor (LiDAR, SAR/InSAR, ETM+, Quickbird) synergy; *Remote Sens. Environ.* **102** 63–73.

Hyde P, Nelson R, Kimes D and Levine E 2007 Exploring LiDAR–RaDAR synergy – predicting aboveground biomass in a southwestern ponderosa pine forest using LiDAR, SAR and InSAR; *Remote Sens. Environ.* **106(1)** 28–38.

Ji L and Gallo K 2006 An agreement coefficient for image comparison; *Photogramm. Eng. Remote Sens.* **72(7)** 823–833.

Kale M P, Ravan S A, Roy P S and Singh S 2009 Patterns of carbon sequestration in forests of Western Ghats and study of applicability of remote sensing in generating carbon credits through afforestation/reforestation; *J. Indian Soc. Remote Sens.* **37** 457–471.

Kumar R, Gupta S R, Singh S, Patil P and Dhadhwal V K 2011 Spatial distribution of forest biomass using remote sensing and regression models in northern Haryana, India; *J. Ecol. Environ. Sci.* **37** 37–47.

Kumar P, Sharma L K, Pandey P C, Sinha S and Nathawat M S 2013 Geospatial strategy for tropical forest-wildlife reserve biomass estimation; *IEEE J. Sel. Topics Appl. Earth Observ.* **6(2)** 917–923.

Kuplich T M, Curran P J and Atkinson P M 2005 Relating SAR image texture to the biomass of regenerating tropical forests; *Int. J. Remote Sens.* **26** 4829–4854.

Lu D 2005 Aboveground biomass estimation using Landsat TM data in the Brazilian Amazon; *Int. J. Remote Sens.* **26(12)** 2509–2525.

Lu D 2006 The potential and challenge of remote sensing-based biomass estimation; *Int. J. Remote Sens.* **27** 1297–1328.

Mbaabu P R, Hussin Y A, Weir M and Gilani H 2014 Quantification of carbon stock to understand two different forest management regimes in Kayar Khola watershed, Chitwan, Nepal; *J. Indian Soc. Remote Sens.,* doi: 10.1007/s12524-014-0379-3.

Rosenqvist A, Milne A, Lucas R, Imhoff M and Dobson C 2003 A review of remote sensing technology in support of the Kyoto Protocol; *Environ. Sci. Policy* **6** 441–455.

Sarker M L R 2010 *Estimation of forest biomass using remote sensing*; Ph.D. Thesis, The Hong Kong Polytechnic University, Hong Kong.

Sharma L K, Nathawat M S and Sinha S 2013 Top-down and bottom-up inventory approach for above ground forest biomass and carbon monitoring in REDD framework using multi-resolution satellite data; *Environ. Monit. Assess.* **185** 8621–8637.

Sharma L K, Sinha S, Nathawat M S and Jeganathan C 2014 Uses of multi-polarized ALOS PALSAR data for biomass assessment of tropical forests: A step towards REDD; In: *Remote Sensing and GIS in Environmental Resource Management* (eds) Naithani S and Jeganathan C, New Delhi, India, Gaura Books India Pvt. Ltd., pp. 183–192.

Singh I J, Mizanurahman M and Kushwaha S P S 2006 Assessment of effect of settlements on growing stock in Thano range of Dehradun forest division using RS & GIS; *J. Indian Soc. Remote Sens.* **34(2)** 209–217.

Sinha S and Sharma L K 2013 Investigations on potential relationship between biomass and surface temperature using thermal remote sensing over tropical deciduous forests; *Research & Reviews: J. Space Sci. Technol.* **2(3)** 13–18.

Sinha S, Sharma L K and Nathawat M S 2013 Integrated geospatial techniques for land-use/land-cover and forest mapping of deciduous Munger forests (India); *Universal J. Environ. Res. Technol.* **3(2)** 190–198.

Sinha S, Sharma L K and Nathawat M S 2015a Improved land-use/land-cover classification of semi-arid deciduous forest landscape using thermal remote sensing; *Egypt. J. Remote Sens. Space Sci.* **18(2)** 217–233.

Sinha S, Jeganathan C, Sharma L K and Nathawat M S 2015b A review of radar remote sensing for biomass estimation; *Int. J. Environ. Sci. Technol.* **12(5)** 1779–1792.

Sinha S, Sharma L K, Jeganathan C, Nathawat M S, Das A K and Mohan S 2015c Efficacy of InSAR coherence in tropical forest remote sensing in context of REDD; *Int. J. Adv. Remote Sensing, GIS & Geography* **3(1a)** 38–46.

Sinha S, Pandey P C, Sharma L K, Nathawat M S, Kumar P and Kanga S 2014 Remote estimation of land surface temperature for different LULC features of a moist deciduous tropical forest region; In: *Remote Sens. Appl. Environ. Res.* (Part 1) (eds) Srivastava P K, Mukherjee S, Gupta M and Islam T, Switzerland, Springer International Publishing, pp. 57–68.

Wollersheim M, Collins M J and Leckie D 2011 Estimating boreal forest species type with airborne polarimetric synthetic aperture radar; *Int. J. Remote Sens.* **32(9)** 2481–2505.

MS received 25 September 2014; revised 8 January 2016; accepted 18 January 2016

Corresponding editor: Pradeep Kumar Thapliyal